GEOPHYSICAL SIGNAL AND IMAGE PROCESSING

The science of geophysics is concerned with the application of principles from physics to the study of the earth. Exploration geophysics involves the investigation of properties of the subsurface layers of the earth by taking measurements at or near the earth's surface. Processing and analysis of these measurements may reveal how the physical properties of the earth's interior vary vertically and laterally. Information of this type is extremely important in the search for hydrocarbons, minerals, and water in the earth. This article summarizes some of the basic results that deal with the application of signal and image processing techniques to the field of exploration geophysics, specifically as it relates to the search for hydrocarbons.

Hydrocarbons are typically found in association with sedimentary sequences in major sedimentary basins in the earth. Thus scientific methods for hydrocarbon exploration depend heavily on our ability to image the earth's subsurface geological structures down to about 12,000 m. Potential hydrocarbon deposits, in the form of petroleum or natural gas, are often associated with certain geological formations such as faults, anticlines, salt domes, stratigraphic traps, and others (Fig. 1). Such formations may be detected on a seismic image, also called a seismic section, only if sophisticated data acquisition and processing methods are used to generate this image.

One of the most popular and successful methods for imaging the earth's subsurface is the seismic exploration method. This method involves generating a disturbance of the surface of the earth by means of the detonation of an explosive charge placed either on the ground, in the case of land exploration, or in water, in the case of offshore marine exploration (Fig. 2). The resulting ground motion propagates downwards inside the earth, gets reflected at the various interfaces of the geological strata, and finally is recorded as a time series, or trace, by sensors placed at some distance from the source of the disturbance. An example of many such traces placed side by side is shown in Fig. 3.

Geophysical signal processing is a field which deals primarily with computer methods for analyzing and filtering a large number of such time series for the purpose of extracting the information necessary to develop an image of the subsurface layers (or geology) of the earth (1–12). In order to give the reader an idea about the volume of geophysical data available for processing, it is estimated that in the 1990s, on the average, approximately 2 million traces are recorded everyday for the purpose of exploring for petroleum and natural gas. Thus careful processing of this enormous amount of data must take advantage of the state of the art in computer technology and make full use of the most advanced techniques in digital signal and image processing.

SEISMIC DATA GENERATION AND ACQUISITION

The first step in any application of a geophysical data-processing method is to understand the process by which the signals to be processed have been generated and recorded. Seismic data for imaging the subsurface layers of the earth down to possibly 12,000 m, are typically generated by a source of seismic energy and recorded by an array of sensors placed on the surface of the earth at some distance from the source. There are several types of seismic sources. The most common are dynamite explosives or vibroseis for land data, or air guns for offshore marine data. Land dynamite explosives and marine air guns, which inject a bubble of highly compressed air into the water, are short-duration (about 0.5 s or less) sources, usually referred to as *wavelets* (see Fig. 4). Vibroseis land sources, on the other hand, are long-duration (typically 8 s or more) low-amplitude sinusoidal waveforms whose frequency varies continuously from about 10 Hz to 80 Hz. The sweep signal is matched filtered to give the equivalent of a short duration correlation function for the outgoing signal. The waveform created by the seismic source propagates downward into the earth, gets reflected, and returns to the surface carrying information about the subsurface structure. Each sensor on the receiving array is a device that transforms the reflected seismic energy into an electrical signal. In the case of land data, recording is done by a geophone, which typically measures particle velocity. In the case of marine data, recording is done by a hydrophone, which typically measures pressure. The recording of every sensor (geophone or hydrophone) is a time series called a *seismic trace.* Each trace may consist of 1,000 to 12,000 samples of data representing 4 s to 6 s of earth motion sampled at periods which could vary anywhere between 0.5 ms and 8 ms. Typical spacing between the sensors is 10 m to 200 m.

The recorded traces can then be sorted so that all traces corresponding to some criterion, such as common-shot-point or common-midpoint, are displayed side-by-side to form what is known as a *shot gather.* Several source–receiver configurations for recording/sorting seismic traces are illustrated in Fig. 5. A sample common-midpoint (*CMP*) shot gather is shown in Fig. 3. A seismic survey typically consists of a large number of shot gathers collected by moving the combination of source and array of receivers along specified survey lines and repeating the data collection process (see Fig. 2). The ultimate goal of geophysical signal processing is to extract information on the physical properties and construct an image of the subsurface structure of the earth by processing these recorded data. Until about the mid-1980s, emphasis was mostly on 2-D imaging along specified survey lines. However, the advent of very powerful data acquisition, storage, and processing capabilities has made it possible to construct 3-D images of subsurface structures (12). Most of the geophysical signal processing work in the mid-1990s and beyond has been focused on 3-D imaging. Surveys that yield 3-D data, however, are more complicated and costly than those that yield 2-D data. For example, 3-D surveys normally utilize methods in which seismic sensors are distributed along several parallel lines and the seismic sources along other lines, hence building a dense array of seismic data. A typical 3-D survey could involve collecting anywhere between several hundred thousands to a few millions traces (12).

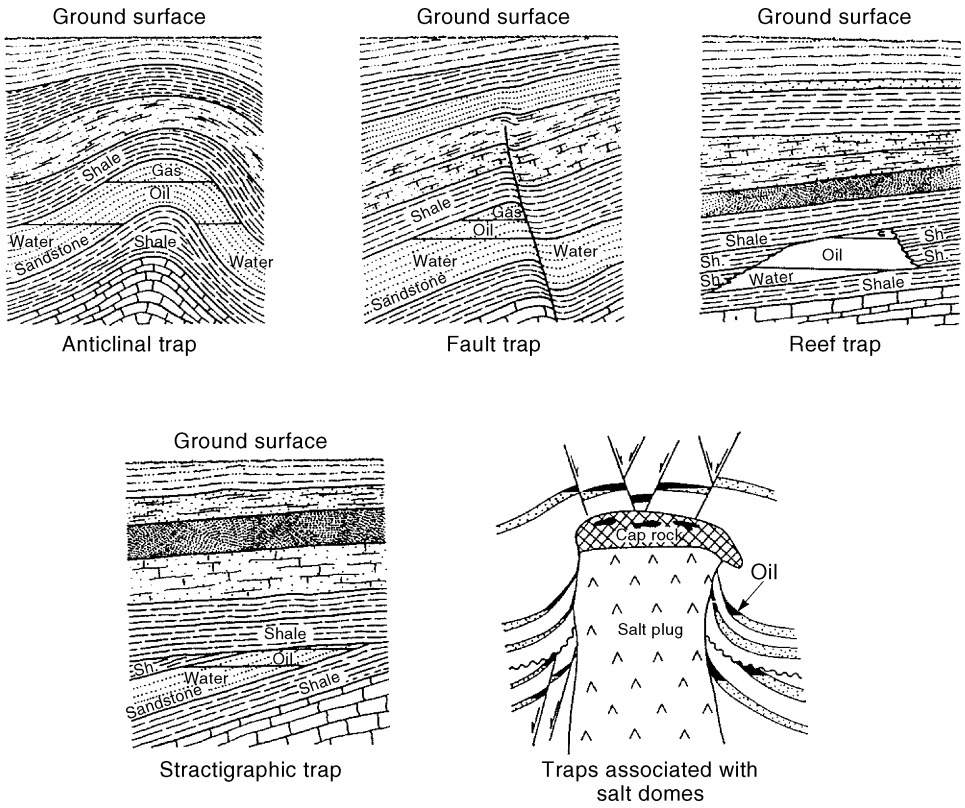

Figure 1. Some geological formations associated with hydrocarbon deposits (2, 5).

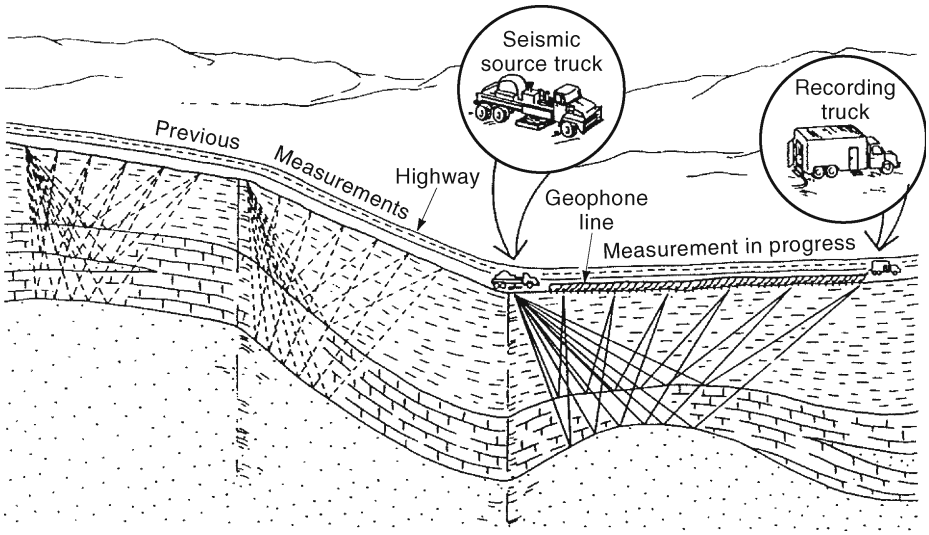

Figure 2. A typical land seismic data acquisition experiment (9).

SEISMIC WAVE PROPAGATION

A seismic wave propagates outwards from the source at a velocity that is typically determined by the physical properties of the propagation medium (surrounding rocks). Seismic rays are thin pencils of seismic energy traveling along raypaths that are perpendicular to the wavefronts. At the interface between two rock layers, there is a change in the physical properties of the media, which results in a change in the propagation velocity. When encountering such an interface, the energy of an incident seismic wave is partitioned into a reflected wave and a transmitted wave. The relative amplitudes of these waves are determined by the velocities and densities of the two layers. Thus, in order to understand the nature of the recorded seismic data, it is essential to understand the propagation mechanism of a seismic signal through a multilayered medium. Note that, as mentioned earlier, in the case of land seismic data, a geophone records vertical displacement velocity, while in the case of marine data, a hydrophone records water pressure.

Consider a simple model of the earth, which consists of a horizontally layered medium (8) where the seismic propagation velocity $\alpha(z)$ and medium density $\rho(z)$ vary only as a function of depth z. In the case of land data, it is known that the vertical stress component $\sigma(z, t)$ is related to vertical displacement velocity $v(z, t)$ by the standard equation

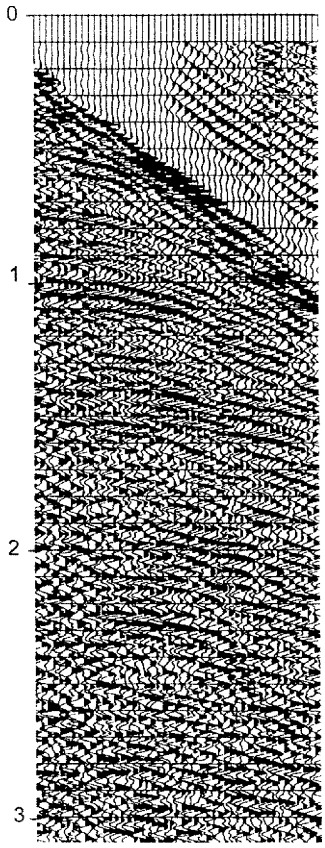

Figure 3. An example of a common depth point (*CDP*) shot gather.

of motion

$$\frac{\partial \sigma}{\partial z} = \rho \frac{\partial v}{\partial t} \tag{1}$$

and Hooke's law

$$\frac{\partial \sigma}{\partial t} = \rho \alpha^2 \frac{\partial v}{\partial z} \tag{2}$$

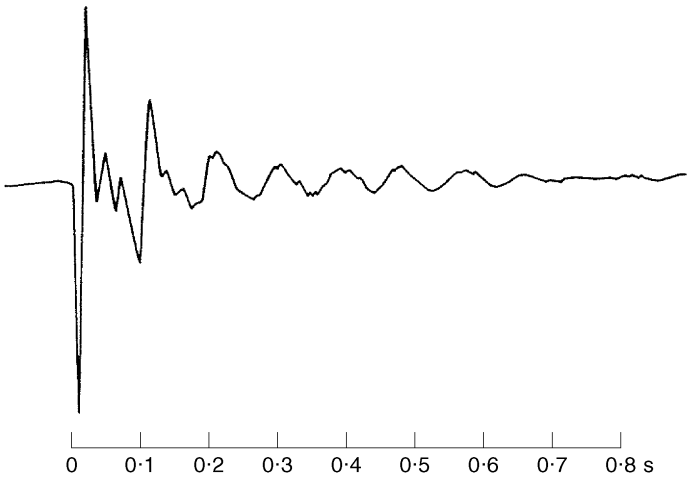

Figure 4. An example of a marine, single air gun, wavelet.

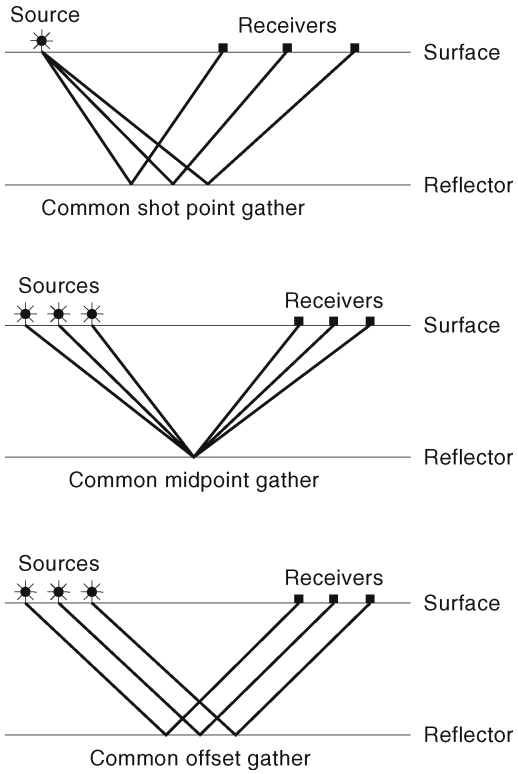

Figure 5. Various source–receiver configurations.

In the Fourier transform domain, these expressions are written as

$$\frac{\partial S}{\partial z} = -j\omega\rho V \tag{3}$$

$$\frac{\partial V}{\partial z} = -j\omega \frac{1}{\rho \alpha^2} S \tag{4}$$

where $S(z, \omega)$ and $V(z, \omega)$ are the Fourier transforms of $\sigma(z, t)$ and $v(z, t)$, respectively. The propagating waveform can be decomposed into its upcoming and downgoing components

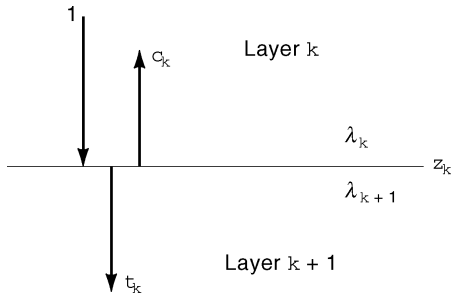

Figure 6. Reflection and transmission coefficients at interface z_k.

U and D using the linear transformation

$$\begin{bmatrix} U \\ D \end{bmatrix} = \frac{1}{2\lambda}\begin{bmatrix} 1 & \lambda \\ -1 & \lambda \end{bmatrix}\begin{bmatrix} S \\ V \end{bmatrix} \tag{5}$$

where $\lambda(z) = \rho(z)\alpha(z)$ is the acoustic impedance. Combining Eq. (5) with Eqs. 4, it can be shown that U and D must satisfy the equations

$$\frac{\partial U}{\partial z} = -\frac{j\omega}{\alpha}U + \gamma(z)(U - D) \tag{6a}$$

$$\frac{\partial D}{\partial z} = +\frac{j\omega}{\alpha}D + \gamma(z)(-U + D) \tag{6b}$$

In the above expressions $\gamma(z)$ is the reflectivity function, which is related to the acoustic impedance $\lambda(z)$ by the expression:

$$\gamma(z) = -\frac{1}{2}\frac{d\ln\lambda(z)}{dz} \tag{7}$$

The above equations can be used to derive synthetic seismograms at any depth. As such, they are necessary prerequisites for solving the inverse problem where the requirement is to determine the reflectivity function from the available seismogram.

If one applies the boundary conditions at the interface between the kth and $k + 1$st layers, as illustrated in Fig. 6, the reflectivity coefficient c_k and transmission coefficient t_k at the interface z_k can be expressed as:

$$c_k = \frac{\lambda_k - \lambda_{k+1}}{\lambda_k + \lambda_{k+1}} \quad \text{and} \quad t_k = \frac{2\lambda_{k+1}}{\lambda_k + \lambda_{k+1}} \tag{8}$$

where λ_k is the acoustic impedance above the interface and λ_{k+1} is the acoustic impedance below the interface. The seismic trace $s(t)$ recorded at the surface is often modeled as a convolution of the source waveform $w(t)$ and a reflectivity function $r(t)$,

$$s(t) = r(t)^* w(t) \tag{9}$$

The reflectivity function $r(t)$ is related to $\lambda(z)$ by observing that two-way travel time t is related to depth z through the seismic propagation velocity.

DETERMINATION OF SEISMIC PROPAGATION VELOCITY

The recorded seismic trace can be processed to estimate the travel times of the reflected ray paths from the source to the receiver. If one knows the velocity distribution as a function of depth between the surface and reflecting planes, the travel times information can be transformed into information on the depths of the reflecting boundary planes. In order to illustrate how this is done, consider the simple model of a single horizontal reflector at a depth z beneath a homogeneous layer with constant velocity V, as shown in Fig. 7. This simple case will probably never occur in practice, but its understanding will make it easier to understand the more complicated cases that are encountered in real situations. Using simple triangle geometry, the travel time from the source, to the reflector, to a receiver at a distance x from the source can be easily computed as

$$t_x = \frac{\sqrt{x^2 + 4z^2}}{V} \tag{10}$$

This expression can be rewritten in the form

$$t_x^2 = t_o^2 + \frac{x^2}{V^2} \tag{11}$$

where $t_0 = 2z/V$ is the two-way travel time obtained from Eq. (10) by setting $x = 0$. This is called the *zero-offset* travel time and corresponds to a hypothetical source–receiver combination placed exactly at the common-midpoint (CMP). The above expression shows that the relationship between t_x and x is hyperbolic, as illustrated in Fig. 8. The difference in travel time between a ray path arriving at an offset distance x and one arriving at zero-offset is called normal move-out (*NMO*). For cases where offset is much smaller than depth (i.e., $x < z$), which is normally the case in practice, Eq. (11) can be approximated as follows:

$$t_x \approx t_0\left\{1 + \frac{x^2}{2V^2t_0^2}\right\} \tag{12}$$

and NMO can be expressed as:

$$\Delta t_x = t_x - t_0 \approx \frac{x^2}{2V^2t_0} \tag{13}$$

The above expression can be rearranged as follows:

$$V = \frac{x}{\sqrt{2t_0\,\Delta t_x}} \tag{14}$$

which means that the velocity of the medium above the reflector can be computed from knowledge of the NMO Δt_x and the zero-offset travel time t_0. In practice, however, this calculation is made using a large number of reflected ray paths to obtain a statistical average of the velocity. As mentioned earlier, once t_0 is known, the depth of the reflector can be computed as $z = Vt_0/2$.

The above analysis may be easily extended to the case of a multilayer medium, as illustrated in Fig. 9. In this case, it can be shown that the two-way travel time of the ray path reflected from the nth interface at a depth z is given by

$$t_{x,n}^2 = t_{0,n}^2 + \frac{x^2}{V_{\text{rms},n}^2} \tag{15}$$

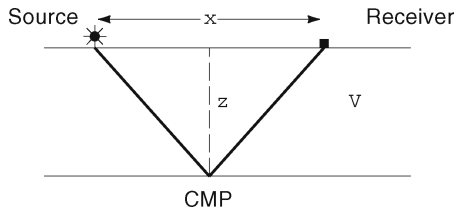

Figure 7. Travel time versus offset.

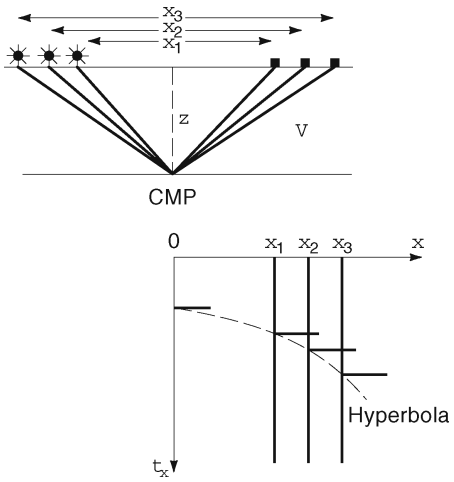

Figure 8. Travel time versus offset.

where $t_{0,n}$ is the zero-offset two-way travel time down to the nth layer, and $V_{\mathrm{rms},n}$ is the root-mean-square velocity of the section of the earth down to the nth layer. The expression for $V_{\mathrm{rms},n}$ is

$$V_{\mathrm{rms},n} = \sqrt{\frac{1}{t_{0,n}} \sum_{i=1}^{n} V_i^2 \tau_i} \tag{16}$$

where V_{i} is the interval velocity of the ith layer and τ_{i} is the one-way travel time of the reflected ray through the ith layer. As in the single reflector case, the NMO for the nth reflector can be approximated as

$$\Delta t_{x,n} \approx \frac{x^2}{2V_{\mathrm{rms},n}^2 t_{0,n}} \tag{17}$$

and this expression can be used to compute the rms velocity value of the layers above the reflector. Once, the rms velocities down to different reflectors have been determined, the interval velocity V_{n} of the nth layer can be computed using the formula (known as Dix' formula)

$$V_n = \sqrt{\frac{V_{\mathrm{rms},n}^2 t_n - V_{\mathrm{rms},n-1}^2 t_{n-1}}{t_n - t_{n-1}}} \tag{18}$$

where $V_{\mathrm{rms},n}$ and $V_{\mathrm{rms},n-1}$ are the rms velocities for layers n and $n-1$, respectively, and t_{n} and $t_{\mathrm{n-1}}$ are the corresponding two-way zero-offset travel times (5).

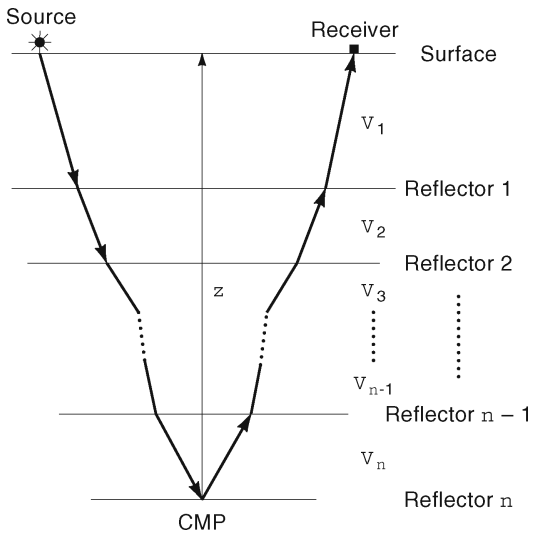

Figure 9. Ray path from source to receiver in a multilayered medium.

STACKING AND VELOCITY ANALYSIS

As mentioned earlier, the most common configuration for collecting and arranging seismic data is the common-midpoint (CMP) reflection profiling shown in Fig. 8. A typical CMP gather is shown in Fig. 3. It is important to point out that a CMP gather represents the best possible data-sorting configuration for using Eq. (15) to estimate seismic velocities from the effects of NMO. To illustrate how this is done, assume that one wishes to estimate the velocity at a given zero-offset time $t_{0,j}$ (where j refers to a sample position on the zero-offset trace). For each value of rms velocity $V_{\mathrm{rms},j}$ that may be guessed, there is a hyperbola defined by Eq. (15). The sum (stack) of the trace samples falling on this hyperbola can therefore be computed and a measure of coherent energy (the square of the sum) can be determined as illustrated in Fig. 10. The hyperbola that produces the maximum coherent energy represents the best fit to the data and the corresponding velocity represents the best estimate of the rms velocity at time $t_{0,j}$. This velocity, denoted by $V_{\mathrm{s},j}$, is called the *stacking velocity* at time $t_{0,j}$. If this process is repeated for all possible sample locations j, a three-dimensional plot of coherent energy as a function of velocity and time on the zero-offset trace can then be produced. An example of such a plot is shown in Fig. 11. The peaks on this, what is often referred to as "velocity spectrum" are used to determine a stacking velocity profile versus two-way travel time. This velocity profile can be used to perform NMO corrections for all times $t_{0,j}$. Interval velocities can then be calculated from the stacking velocities by means of Dix' formula [Eq. (18)].

Once accurate velocity information is available, it becomes possible to correct for the effects of NMO. This is achieved by shifting the samples on each trace (i.e., flatten the hyperbola that corresponds to the stacking velocity) to obtain an estimate of a corresponding zero-offset trace at the CMP of the gather. If done correctly, all reflections coming from the same horizontal reflector will line-up at the same zero-offset time on the corrected traces, as illus-

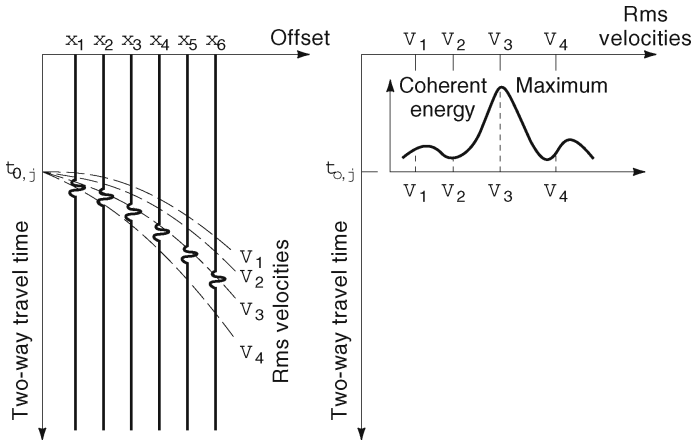

Figure 10. Computation of stacking velocity from a CDP gather.

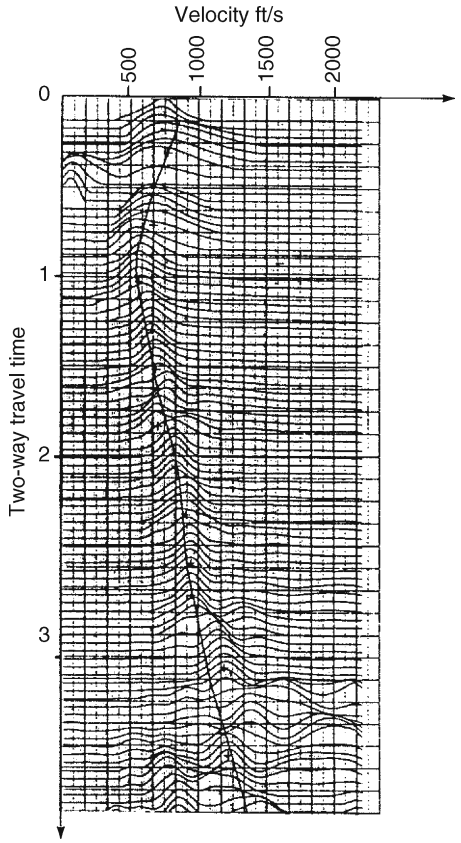

Figure 11. An example of a velocity spectrum plot.

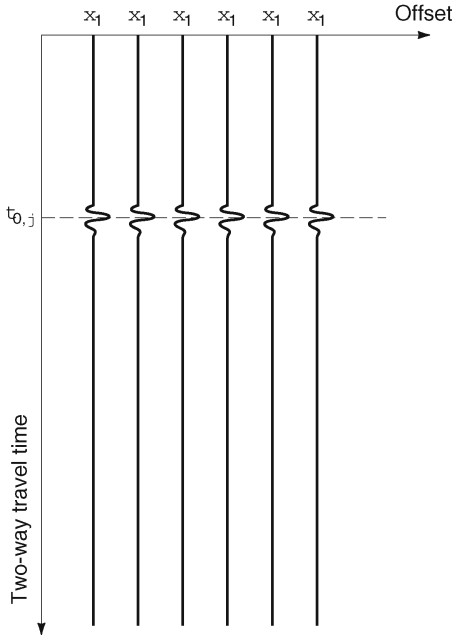

Figure 12. NMO corrected traces of data in Fig. 10.

trated in Fig. 12. Other coherent events such as multiples, which have different rms velocities, and random noise, will not be aligned. These traces can therefore be summed algebraically to produce one trace, that corresponds to the CMP, in which the reflected aligned events have been reinforced and the other effects reduced. This process is called *stacking* and the output is called a *stacked trace.* When a large number of stacked traces corresponding to successive common-midpoints are placed side-by-side, the resulting image is called a stacked seismic section. An example of a stacked seismic section is shown in Fig. 13. A stacked section represents an image showing geologic formations that would be exposed if the earth were to be sliced along the line of the survey that produced the section.

SEISMIC DECONVOLUTION

A very important step in geophysical signal processing that is often (but not always) performed prior to stacking is deconvolution. Deconvolution is a process by which the effect of the source waveform is compressed so as to improve temporal resolution. In order to understand the concept of deconvolution, go back to the basic model described earlier in Eq. (9), which represents a seismic trace $s(t)$ as a convolution of a source waveform $w(t)$ and a reflectivity sequence $r(t)$; that is, $s(t) = r(t)*w(t)$. Note that, for the sake of brevity, the effects of random noise, which are almost always present, have not been included in this model. The reflectivity sequence $r(t)$ is also called the earth impulse response. It represents what would be recorded if the source waveform were purely an impulse function $\delta(t)$ (a spike). Recall that the reflectivity sequence $r(t)$ contains informa-

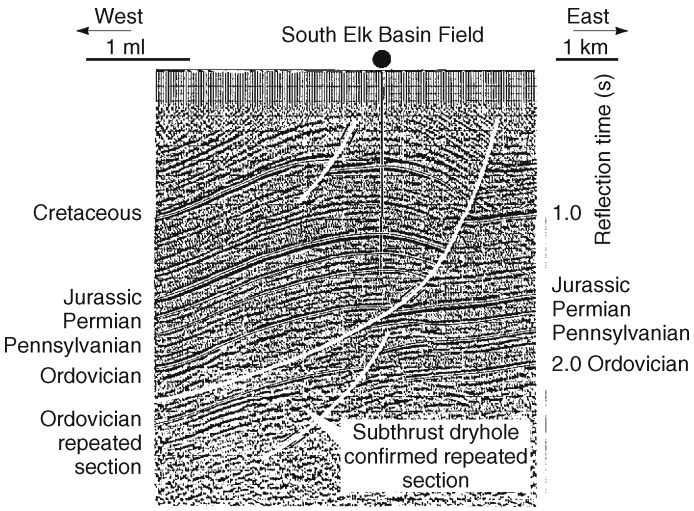

Figure 13. An example of a stacked seismic section. Note the folded and thrust-faulted structure (9).

tion about the subsurface characteristics of the earth. The source waveform $w(t)$ is therefore a blurring (or smearing) function that makes it difficult to recognize the reflectivity sequence by directly observing the trace $s(t)$. If it were possible to generate a source waveform that corresponds to an impulse function $\delta(t)$, then, except for the effects of random noise, each trace will indeed be a recording of the reflectivity sequence. Generating a seismic source that is a close approximation of the impulse function (i.e., where most of the energy is concentrated over a very short interval of time) has been a dilemma that has, for years, received considerable attention in the geophysical industry and related literature.

Estimating the reflectivity sequence $r(t)$ from $s(t) = r(t)*w(t)$ has probably been one of the most studied problems in geophysical signal processing and much research effort has been devoted to the development of methods for carrying out this operation. Among the most popular such methods are the optimum Wiener filtering, predictive deconvolution, spiking deconvolution, homomorphic deconvolution, and numerous others (15). For the sake of conciseness, the Wiener filtering method will be discussed in some detail, while the others will be briefly summarized.

Wiener Filtering Method

Assume that one has a signal $x(t)$ and that one wishes to apply a filter $f(t)$ to this signal in order to make it resemble a desired signal $d(t)$. The Wiener filtering method, illustrated in Fig. 14, involves designing the filter $f(t)$ so that the least-squares error between the actual output $y(t) = x(t)*f(t)$ and the desired outputs $d(t)$ is minimized. For simplicity, the steps for deriving the filter $f(t)$ (for the deterministic case) will be carried out using discrete rather than continuous signals and with matrix notation. Assume that the input sequence has n samples $x_0, x_1, \ldots, x_{n-1}$ and the unknown filter has m samples $f_0, f_1, \ldots, f_{m-1}$ and let

$$\boldsymbol{x} = \begin{bmatrix} x_0 \\ x_1 \\ . \\ . \\ x_{n-1} \end{bmatrix} \quad \text{and} \quad \boldsymbol{f} = \begin{bmatrix} f_0 \\ f_1 \\ . \\ . \\ f_{m-1} \end{bmatrix} \tag{19}$$

be the n- and m-dimensional vectors of these samples, respectively. The actual output vector which is the convolution of the input sequence and the filter coefficients can be expressed in matrix form as:

$$\begin{bmatrix} y_0 \\ y_1 \\ . \\ . \\ . \end{bmatrix} = \begin{bmatrix} x_0 & 0 & . & . & \\ x_1 & x_0 & 0 & . & . \\ x_2 & x_1 & x_0 & 0 & . \\ . & x_2 & x_1 & x_0 & 0 \\ . & . & x_2 & x_1 & x_0 \end{bmatrix} . \begin{bmatrix} f_0 \\ f_1 \\ . \\ . \\ f_{m-1} \end{bmatrix} \tag{20}$$

or

$$\boldsymbol{y} = \boldsymbol{X}.\boldsymbol{f} \tag{21}$$

where X is an $(n + m - 1) \times m$ lower diagonal matrix whose entries are derived from the input sequence, and y is the $(n + m - 1)$ vector of actual output samples. The error vector can now be defined as

$$\boldsymbol{e} = \boldsymbol{y} - \boldsymbol{d} = \boldsymbol{X}\boldsymbol{f} - \boldsymbol{d} \tag{22}$$

where d is the vector of desired output samples. The optimum filter is derived by minimizing the norm of the error, that is,

$$e_r = \|\boldsymbol{X}\boldsymbol{f} - \boldsymbol{d}\|^2 \tag{23}$$

It can be easily shown that the optimum vector f^* that minimizes e_r is the solution of the linear matrix equation

$$(\boldsymbol{X}'\boldsymbol{X})\boldsymbol{f}^* = \boldsymbol{X}'\boldsymbol{d} \tag{24}$$

Note that upon computing the entries of the $m \times m$ matrix $X'X$, the above equation can be written as:

$$\begin{bmatrix} \phi_0 & \phi_1 & \phi_2 & . & \phi_{m-2} & \phi_{m-1} \\ \phi_1 & \phi_0 & \phi_1 & \phi_2 & . & \phi_{m-2} \\ \phi_2 & \phi_1 & \phi_0 & \phi_1 & \phi_2 & . \\ . & \phi_2 & \phi_1 & \phi_0 & \phi_1 & \phi_2 \\ \phi_{m-2} & . & \phi_2 & \phi_1 & \phi_0 & \phi_1 \\ \phi_{m-1} & \phi_{m-2} & . & \phi_2 & \phi_1 & \phi_0 \end{bmatrix} . \begin{bmatrix} f_0^* \\ f_1^* \\ f_2^* \\ . \\ . \\ f_{m-1}^* \end{bmatrix} = \begin{bmatrix} g_0 \\ g_1 \\ g_2 \\ . \\ . \\ g_{m-1} \end{bmatrix} \tag{25}$$

where ϕ_i are the autocorrelation lags of the input signal and g_i are the crosscorrelations between the input signal

and the desired output; that is,

$$\phi_{i-j} = \sum_k x_{k-i}x_{k-j} \qquad \text{and} \qquad g_i = \sum_k x_{k-i}d_k \tag{26}$$

It is important to mention that the autocorrelation matrix is Toeplitz in nature, and hence the optimum filter coefficients can be calculated using the Levinson recursion algorithm (3). Also, note that in the above analysis, the only requirement for the derivation of the filter coefficients is an a priori knowledge of the autocorrelation coefficients of the input signal and the crosscorrelation coefficients of the input signal with the desired output signal. Clearly, the filter length m needs to be specified a priori and cannot be changed during or after the computation of the filter coefficients without repeating the entire computations.

Prediction Error Filtering

A special case of the above derivation is when the desired output signal is an advanced version of the input signal; that is, $d_k = x_{k+p}$. In such a case, the filter is called a p-step ahead predictor. That is, at sample k, it predicts x_{k+p} from past values of the input. The derivation of such a filter is essentially the same as described above except that x_{k+p} should be used in place of d_k in Eq. (26). That is,

$$g_i = \sum_k x_{k-i}x_{k+p} = \phi_{p+i} \tag{27}$$

The desired output in this case is the predictable part of the input series. This, for example, could include events such as multiples. The error signal contains the unpredictable part, which is the uncorrelated reflectivity sequence that we are trying to extract from the measurements. Of special interest is the one step ahead predictor ($p = 1$). In that case, it can be shown that the minimum error can be added as an additional unknown to Eq. (24), which can then be solved for, along with the filter coefficients. Also, the error series (or reflectivity sequence) can now be computed using Eq. (22) as:

$$\boldsymbol{e} = \boldsymbol{X}\boldsymbol{h} \tag{28}$$

where the vector $h = [1 \; -f^*_0 \; -f^*_1 \; .. \; -f^*_{m-1}]'$. It should be noted that this (deconvolution) approach for estimating the reflectivity sequence, also known as predictive deconvolution, is based on two important assumptions. First, the reflectivity sequence represents a random series (i.e., no predictable patterns) and second the wavelet must be minimum phase.

Spiking Deconvolution Method

Assume that it is possible to find a filter $f(t)$ such that when applied to the seismic source waveform $w(t)$, one gets the impulse function $\delta(t)$; that is,

$$w(t)^* f(t) = \delta(t) \tag{29}$$

Then, if one applies this filter to the seismic trace $s(t) = r(t)^*w(t)$, one gets:

$$\begin{aligned} s(t)^* f(t) &= r(t)^* w(t)^* f(t) \\ &= r(t) \end{aligned} \tag{30}$$

which means that it would be possible to recover the reflectivity sequence $r(t)$. The filter $f(t)$, if it exists, is called the inverse filter of the seismic source $w(t)$. The nature of this inverse filter can also be examined in the frequency domain. Taking the Fourier transform of both sides of Eq. (29), one obtains

$$\boldsymbol{W}(\omega)\boldsymbol{X}(\omega) = \boldsymbol{1} \tag{31}$$

where

$$\boldsymbol{W}(\omega) = |W(\omega)|e^{j\Phi_w(\omega)}, \quad \text{and} \quad \boldsymbol{X}(\omega) = |X(\omega)|e^{j\Phi_x(\omega)} \tag{32}$$

From this, it follows that:

$$|X(\omega)| = \frac{1}{|W(\omega)|} \qquad \text{and} \qquad \Phi_x(\omega) = -\Phi_w(\omega) \tag{33}$$

This means that the amplitude spectrum of the inverse filter is the inverse of that of the seismic wavelet and the phase spectrum of the inverse filter is the negative of that of the seismic wavelet. A problem therefore will immediately arise if the amplitude spectrum of the wavelet has frequencies at which it is equal to zero. Clearly, at those frequencies the amplitude spectrum of the inverse filter becomes infinite (or undefined) and hence the filter will be unbounded in the time domain. Similar problems will also arise even if at some frequencies the values of the amplitude spectrum of $w(t)$ are very small. Clearly, using Eq. (33) for calculating the inverse filter $f(t)$ is not feasible in almost all realistic applications.

Suppose instead, the Wiener filtering approach is used and a filter $f(t)$ is designed which, when applied to the source waveform $w(t)$, will produce an output which is as close as possible to a desired impulse function (a spike). In other words, referring to the Wiener Filtering approach discussed earlier, suppose the source waveform has n samples, $w_0, w_1, \ldots, w_{n-1}$, the unknown filter has m samples f_0, $f_1, \ldots, f_{m-1}$, and the desired output is an impulse which has $n + m - 1$ samples $\delta_0, \delta_1, \ldots, \delta_{n+m-1}$ and whose entries are all 0 except for 1 at one location; say the jth location. Then the filter coefficients are determined so as to minimize the error function:

$$e_r = \|W\boldsymbol{f} - \boldsymbol{\delta}\|^2 \tag{34}$$

where

$$\boldsymbol{W}\boldsymbol{f} = \begin{bmatrix} w_0 & 0 & 0 & . & . \\ w_1 & w_0 & 0 & . & . \\ w_2 & w_1 & 2_0 & 0 & . \\ . & w_2 & w_1 & w_0 & 0 \\ . & . & w_2 & w_1 & w_0 \end{bmatrix} \begin{bmatrix} f_0 \\ f_1 \\ . \\ . \\ f_{m-1} \end{bmatrix} \qquad \text{and} \qquad \tilde{\delta} = \begin{bmatrix} \delta_0 \\ \delta_1 \\ . \\ . \\ . \end{bmatrix} \tag{35}$$

As discussed in the derivation of the Wiener Filter, and using Eq. (24), the optimum vector that minimizes e_r is given by the expression:

$$\boldsymbol{f}^* = (W'W)^{-1}W'\boldsymbol{\delta} \tag{36}$$

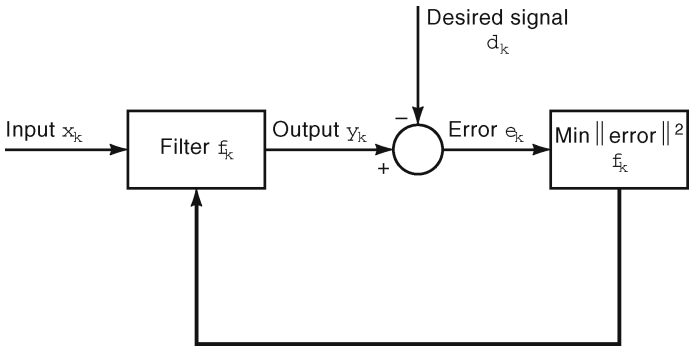

Figure 14. The Wiener filtering method.

This can be written as:

$$\boldsymbol{f}^* = \begin{bmatrix} \phi_0 & \phi_1 & \phi_2 & \cdot & \cdot & \phi_{m-1} \\ \phi_1 & \phi_0 & \phi_1 & \phi_2 & \cdot & \cdot \\ \phi_2 & \phi_1 & \phi_0 & \phi_1 & \phi_2 & \cdot \\ \cdot & \phi_2 & \phi_1 & \phi_0 & \phi_1 & \phi_2 \\ \cdot & \cdot & \phi_2 & \phi_1 & \phi_0 & \phi_1 \\ \phi_{m-1} & \cdot & \cdot & \phi_2 & \phi_1 & \phi_0 \end{bmatrix}^{-1} \begin{bmatrix} g_0 \\ g_1 \\ g_2 \\ \cdot \\ \cdot \\ g_{m-1} \end{bmatrix} \tag{37}$$

where ϕ_i are the autocorrelation lags of the source waveform and g_i are the crosscorrelations between the source waveform and the desired output:

$$\phi_{i-j} = \sum_k w_{k-i} w_{k-j} \qquad \text{and} \qquad g_i = \sum_k w_{k-i} \delta_k \tag{38}$$

Note that it is also possible to choose the optimal location j^* of the spike in the δ vector in order to achieve the smallest possible error. This can be done by noting that, when Eq. (36) is substituted in Eq. (34), the minimum value of e_r will reduce to the quadratic expression $e_{\min} = \delta' M \delta$ where M is an $m \times m$ matrix equal to $M = I - W(W'W)^{-1}W'$. Given that the δ vector is all zeroes except for the number 1 in one location, $e_{\min}$ will be smallest when j^* is chosen to correspond to the location of the smallest term on the diagonal of the matrix M.

Homomorphic Deconvolution

In the late 1960s a class of nonlinear systems, called homomorphic systems (16, 17), which satisfy a generalization of the principle of superposition has been proposed. Homomorphic filtering is essentially the use of a homomorphic system to remove an undesired component from a signal. Homomorphic deconvolution involves the use of homomorphic filtering for separating two signals that have been convolved in the time domain. An important aspect of the theory of homomorphic deconvolution is that it can be represented as a cascade of three operations. The following will summarize how this theory can be used to separate the reflectivity sequence $r(t)$ and the source waveform $w(t)$ from the seismic trace $s(t) = r(t)*w(t)$.

The first operation involves taking the Fourier transform of $s(t)$. That is, $S(\omega) = R(\omega)W(\omega)$. The second operation involves taking the logarithm of $S(\omega)$:

$$\log[S(\omega)] = \log[R(\omega)] + \log[W(\omega)] \tag{39}$$

Note that since the Fourier transform is a complex function, it is necessary to define the logarithm of a complex quantity. An appropriate such a definition for a complex function $X(\omega)$ is:

$$\log[X(\omega)] = \log[|X(\omega)|e^{j\Phi_x(\omega)}] = \log|X(\omega)| + j\Phi_x(\omega) \tag{40}$$

In the above expression, the real part, $\log|X(\omega)|$, causes no problem. Problems of uniqueness, however, arise in defining the imaginary part since, $\Phi_x(\omega)$ is defined only to within $\pm\pi$. One approach to dealing with this problem is to require that $\Phi_x(\omega)$ be a continuous odd function of ω. That is, the phase function $\Phi_x(\omega)$ must be unwrapped. It is important to point out that Eq. (39) shows that the multiplication operation in the frequency domain has now been changed to an addition operation in the log-frequency domain. The third operation is to take the inverse Fourier transform of $\log[S(\omega)]$. The resulting function is called the complex cepstrum of $s(t)$. Now if the characteristics of the two signals $r(t)$ and $w(t)$ are such that they appear nonoverlapping in this domain, then they can be separated by an appropriate window function. This operation is essentially the filtering operation. In general, it is very unlikely to have a seismic trace where there is complete nonoverlapping in the complex cepstrum of $s(t)$. However, once this is achieved, the reverse process can be applied on each of the separated signals. That is, Fourier transform, followed by inverse logarithm, followed by inverse Fourier transform. The first applications of homomorphic systems were in the area of speech processing (18). Homomorphic deconvolution of seismic data was introduced by Ulrych (19) in the early 1970s and later on extended by Tribolet (20). It should be pointed out that one of the major problems encountered in using homomorphic deconvolution is the problem of unwrapping of the phase.

CONCLUSION

The field of geophysical signal processing deals primarily with computer methods for processing geophysical data collected for the purpose of extracting information about the subsurface layers of the earth. In this article, some of the main steps involved in acquiring, processing, displaying, and interpreting geophysical signals have been outlined. Clearly, many other important steps have not been covered and considerably more can be said about each of the steps that were covered. For example, ac-

quisition of geophysical data also involves issues in geophone/hydrophone array design and placement, field operations, noise control, and digital recording systems. Processing the data is typically an iterative process which also involves issues in static corrections, multiple suppression, numerous deconvolution applications, migration, imaging beneath complex structures, and F-K filtering, to mention several. Displaying and interpreting geophysical data also involves issues in data demultiplexing and sorting, amplitude adjustments and gain applications, 2-D and 3-D imaging, geological modeling, as well as identification of stratigraphic boundaries and structural features on the final image.

MARWAN A. SIMAAN
University of Pittsburgh,
Pittsburgh, PA

BIBLIOGRAPHY

1. A. I. Levorsen *Geology of Petroleum*, San Francisco: Freeman, 1958.
2. M. B. Dobrin *Geophysical Prospecting*, New York: McGraw-Hill, 1960.
3. J. F. Claerbout *Fundamentals of Geophysical Data Processing*, New York: McGraw-Hill, 1976.
4. E. A. Robinson S. Treitel *Geophysical Signal Analysis*, Englewood Cliffs, NJ: Prentice-Hall, 1980.
5. C. H. Dix *Seismic Prospecting for Oil*, Boston: IHRDC, 1981.
6. M. A. Simaan *Advances in Geophysical Data Processing*, Greenwich, CT: JAI Press, 1984.
7. E. A. Robinson T. S. Durrani *Geophysical Signal Processing*, Englewood Cliffs, NJ: Prentice-Hall, 1986.
8. O. Yilmaz *Seismic Data Analysis: Processing, Inversion, and Interpretation of Seismic Data*, Investigations in Geophysics, No. 10, Tulsa: SEG Press, 2001.
9. L. R. Lines R.T. Newrick *Fundamentals of Geophysical interpretation*, Tulsa: SEG Press, 2004.
10. L. T. Ikelle L. Amundsen *Introduction to Petroleum Seismology*, Investigations in Geophysics, No. 12, Tulsa: SEG Press, 2005.
11. D. K. Butler *Near Surface Geophysics*Investigations in Geophysics, No. 13, Tulsa: SEG Press, 2005.
12. B. L. Biondi, *3D Seismic Imaging*, Investigations in Geophysics, No. 14, Tulsa: SEG Press, 2006.
13. E. S. Robinson C. Coruh *Basic Exploration Geophysics*, New York: Wiley, 1988.
14. B. Ursin K. A. Bertussen Comparison of some inverse methods for wave propagation in layered media, *Proc. IEEE*, **3**: 389–400, 1986.
15. V. K. Arya J. K. Aggarwal *Deconvolution of Seismic Data*, Stroudsburg, PA: Hutchinson & Ross, 1982.
16. A. V. Oppenheim R. W. Schafer T. G. Stockman, Jr. Nonlinear filtering of multiplied and convolved signals, *Proc. IEEE*, **8**: 1264–1291, 1968.
17. A. V. Oppenheim R. W. Schafer *Discrete-Time Signal Processing*, Englewood Cliffs, NJ: Prentice-Hall, 1989.
18. L. R. Rabiner R. W. Schafer *Digital Processing of Speech Signals*, Englewood Cliffs, NJ: Prentice-Hall, 1989.
19. T. Ulrych Application of homomorphic deconvolution to seismology, *Geophysics*, **36** (4): 650–660, 1971.
20. J. M. Tribolet *Seismic Applications of Homomorphic Signal Processing*, Englewood Cliffs, NJ: Prentice-Hall, 1979.